NHMFL REPORTS

The National High Magnetic Field Laboratory

Operated by: FLORIDA STATE UNIVERSITY • UNIVERSITY OF FLORIDA • LOS ALAMOS NATIONAL LABORATORY

WINTER 2000
Volume 7 • No.1

From the Chief Scientist's Desk

Robert Schrieffer

Previewing the 1999 NHMFL Annual Research Review

The laboratory's major Annual Report of Research has just been completed and sent to the printer. It should be available in printed form and on the internet (www.magnet.fsu.edu/publications) in the very near future. We are pleased to use this issue of *NHMFL Reports* to feature some of the exciting work underway at the NHMFL.

1999 once again showed a significant increase in the scope and strength of the research projects in the laboratory. The number of projects increased to 310 from 293, 255, and 239 in previous years. There continues to be increased collaborative research between in-house research staff and external users, some of which is supported by the NHMFL In-House Research program.

The research of the laboratory is broadly distributed across sixteen disciplines, with the largest number of projects being superconductivity (43), semiconductors (37), magnetism and magnetic materials (36), magnetic resonance techniques (35), biology (34), chemistry (24), molecular conductors (24) and heavy fermions (22).

We highlight here just a few topics from several of the areas of research as typical of the overall research program. Many other projects of comparable importance could have been chosen.

Biology

Behavioral and Neural Effects of Static High Magnetic Fields

Houpt, T.A., *FSU, Biological Science*
Smith, J.C., *FSU, Psychology*
Snyder, D. *FSU, Neuroscience*
Jahng, J.W., *Yonsei College of Medicine, Korea, Pharmacology*

Advances in magnetic resonance imaging (MRI) are driving the development of faster and higher resolution MRI machines.

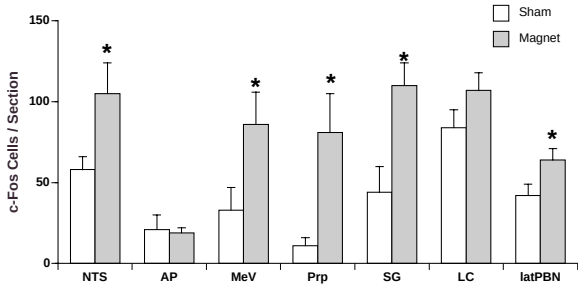

Figure 1. *Exposure to a 9.4 T magnetic field activated neurons in regions of the rat brain sensitive to vestibular and visceral stimulation, as indicated by increased numbers of c-Fos-expressing compared to sham-exposed rats.*

Biology *continued on page 2*

Chemistry

330 to 670 GHz EPR Studies of Canthaxanthin Radical Cation Stabilized on a Silica-Alumina Surface

Konovalova, T.A., *Univ. of Alabama, Chemistry*
Krzystek, J., *NHMFL*
Bratt, P.J., *UF, Chemistry*
Van Tol, J., *NHMFL*
Brunel, L.-C., *NHMFL*
Kispert, L.D., *Univ. of Alabama, Chemistry*

We report the first example of a well-resolved 330-670 GHz EPR spectra of a carotenoid radical cation. At 9-250 GHz the carotenoid radical cation cannot be distinguished from other C-H π-radicals observed in powder and frozen glasses, since its g tensor cannot be resolved at these frequencies. The 330 GHz and higher frequency EPR spectra were resolved into two principal components of the *g* tensor. Spectral simulation indicated this to be the result of *g*-anisotropy where $g_{||}$ = 2.0032 and $g_{\perp}$ = 2.0023. This type of g tensor is consistent with the theory for polyacene π-radical cations, which states that the g tensor becomes cylindrically symmetric with increasing chain length.[1] This also demonstrates that the symmetrical unresolved EPR line at 9 GHz is due to a carotenoid π-radical cation with electron density distributed throughout

Chemistry *continued on page 2*

Biology *cont. from page 1*

Little is known about the sensory or physiological effects of static magnetic fields of high strength on mammals and humans. We have recently discovered that 30 min exposure to a 9.4 T magnetic field has behavioral and neural effects on rat. At the behavioral level, magnetic field exposure induced a conditioned taste aversion (CTA) after pairing with the taste of saccharin. Because CTA has proven to be a sensitive index of visceral malaise, this suggests that the magnetic field may be an aversive stimulus to the rat.

At the neural level, the same exposure induced specific and significant c-Fos immunoreactivity, a marker of neuronal activation, in the rat brainstem. Magnet-exposed rats (n=6) were confined in a Plexiglas tube for 30 min within the 9.4 T magnet. Sham-exposed rats (n=6) were restricted in the same manner for the 30-min period, but not exposed to the magnetic field. One hour later, rats were overdosed with sodium pentobarbital, and transcardially perfused. Brain sections through the medulla and pons were processed for c-Fos. The number of c-Fos-positive cells was quantified in several visceral and stress relays (e.g. nucleus of the solitary tract (NTS), locus ceruleus (LC) and parabrachial nucleus (PBN) and in vestibular nuclei (e.g. the medial vestibular nucleus (MeV), prepositus (Prp), and supragenualis (SG); see Figure 1).

Both the behavioral response and the pattern of c-Fos activation are similar to the effects of vestibular disturbance, such as rotation and motion sickness. Therefore, our working hypothesis is that the magnetic field activates the vestibular apparatus of the inner ear, causing vertigo and CTA acquisition. This is consistent with the self-reports of vertigo and nausea in humans exposed to 4 T magnetic fields. These preliminary findings suggest that CTA and c-Fos expression can be used in an animal model of the behavioral and neural effects of high-strength, static magnetic fields.

Chemistry *cont. from page 1*

the whole chain as predicted by RHF-INDO/SP molecular orbital calculations. The lack of temperature dependence of the EPR linewidths over the range of 5 to 80 K suggests rapid rotation of methyl groups even at 5 K that averages out the proton couplings from three oriented β-protons.

The present work shows that the 330 to 670 GHz EPR measurements are sufficient to resolve the individual *g* tensors components and distinguish carotenoid radical cations from other C-H containing radicals, which have different symmetry.

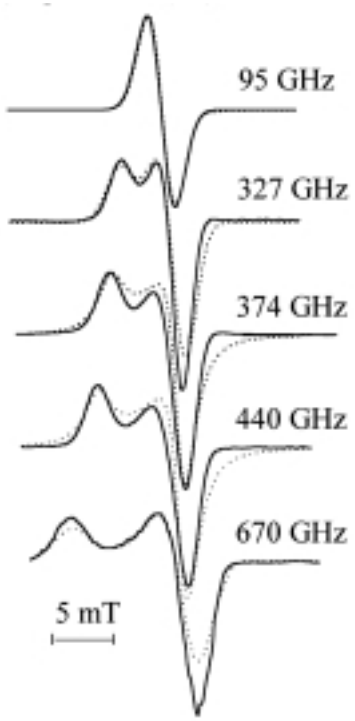

Figure 1. *HF-EPR spectra of canthaxanthin radical cation: (solid) experimental, (dot) simulated.*

[1] Stone, A.J., Mol. Phys., **7**, 309 (1964).

Geochemistry

Parametrization of Trace Element Partitioning on the Mantle Solidus

Salters, V.J.M, *NHMFL, NHMFL/FSU Geological Sciences*
Longhi, J., *Columbia Univ., Lamont-Doherty Earth Observatory*

We have determined experimentally the partitioning of Y, Nb, Ce, Nd, Sm, Er, Yb, Lu, Hf, U, Th, and Pb for garnet, clinopyroxene and orthopyroxene at pressures up to 3.4 GPa. The pressures, temperatures and compositions at which we determined the partitioning is representative of the conditions near the mantle solidus. Most of the new experimental data confirm our previous studies (Salters and Longhi 1999) in terms of both absolute levels of partition coefficients for these elements as well as our first order model to explain the variations. The new data allows further assessment of the compositional and pressure and temperature dependence of the partition coefficients (Ds) and parametrization of the Ds up to 3.4 GPa, although the cause and effect of indiidual parameters are still hard to distinguish. Our highest pressure data shows that the absolute Ds for the heavy REE at higher pressures decreases; D_{Lu} for garnet varies between 4 and 6 at 3.4 GPa, while D_{Lu} reaches values up to 12 at 2.8 GPa. D_{REE} for garnet seems to correlate best with melt structure, measured as non-bridging oxygens (NBO) over tetrahedral

silica (T). The Ds are highest in garnets in equilibrium with the most polymerized melt (lowest NBO/T).

Enough partitioning data is now available to allow a systematic description of the variations of the partition coefficients as a function of pressure, temperature and composition. There are two different ways partitioning behavior can be parametrized:

- Using theory that describes how well the substituting ion "fits" in the crystal lattice (Wood and Blundy 1997). This parametrization describes the crystal chemical controls partitioning as a function of the size of the substituting ion, the optimum size of the site and the rigidity of the crystal lattice.
- Using thermodynamic descriptions for exchange reactions or formation reactions out of melt components. This approach yields information on the enthalpy and entropy a of reaction. In addition first order Margules parameters are used to describe the excess free energy of mixing. This approach is very similar to the one used by Gaetani and Grove (1995).

We found that for both garnet and clinopyroxene best descriptions of the partitioning behavior are made using the thermodynamic descriptions. Multiple lineair regressions using the minimum number of variables produce fits with R^2 values consistently larger than 0.8. Best descriptions of partitioning behavior are found if the melts is parametrized according to Bottinga and Weill (1972). Although these parametrizations are able to model the partition behavior accurately within the composition range of the experiments the thermodynamic constants calculated from these regressions are not always realistic. Partitioning experiments over a wider range of compositions would yield more realistic thermodynamic constants but would not necessarily lead to more accurate predictions of partition coefficients.

Parametrization describing crystal chemical controls as described by Wood and Blundy yields to correlation between observed and predicted partition coefficents with R^2 of less than 0.5. This correlation can be improved significantly if a parametrization is also a function of the melt structure (described as either number of non-bridging oxygens over tetrahedral silicas or as alkalinity of the melt), but this parametrization is still less accurate then the pure thermodynamic approach.

Enough partitioning information is now available to allow assessment of partitioning behavior during melting of garnet peridotite as well as garnet pyroxenite and it can be shown that melts from these two different lithologies have distinctive U-Th, Sm-Nd and Lu-Hf isotope and trace element systematics (Stracke *et al*, 1999). Compared to melts from a garnet-pyroxenite or eclogite, melts from a garnet-peridotite are significantly more enriched in Th compared to U, leading to larger Th-excesses in garnet-peridotite derived melts. Compared to garnet-pyroxenite or eclogite, Lu-Hf fractionation is smaller, and Sm-Nd fractionation is larger during melting of garnet-peridotite. Thus, for similar degrees of melting, garnet-peridotite derived melts have significantly larger Th-excesses, and lower Lu/Hf and Sm/Nd ratios compared to garnet-pyroxenite derived melts. It can be shown that the isotope and trace element variations at Hawaii are incompatible with the presence of garnet pyroxenite in the source of Hawaiian basalts (Stracke *et al*, 1999).

[1] Bottinga and Weill, Am. J. Sci. **272**, 438-475 (1972).
[2] Gaetani and Grove, Geochim. Cosmochim. Acta **59**, 1951-1962 (1995).
[3] Salters and Longhi, Earth Plan. Sci. Lett., **166**, 15-30 (1999)
[4] Stracke *et al*, G^3, 1st Issue, (1999).
[5] Wood and Blundy, Contrib.Mineral. Petrol. **129**, 166-181 (1997).

Kondo / Heavy Fermion Systems

Ultrasound Measurements Near the Metamagnetic Transition in UPt_3

Feller, J., *Univ. of Wisconsin-Milwaukee and Northwestern Univ., Physics*
Ketterson, J.B., *Northwestern Univ., Physics*
Sarma, B.K., *Univ. of Wisconsin-Milwaukee, Physics*

High resolution ultrasonic velocity and attenuation measurements have been performed on a single crystal of UPt_3 at the 33 T mK (dil. fridge) facility at NHMFL, Tallahassee. Figure 1 shows the relative velocity (normalized to zero at zero field) of longitudinal sound in the basal plane (b-axis). The magnetic field is parallel to the b-axis. The metamagnetic transition field is ~20.25 T. At low temperatures (below ~1 K) a second velocity dip develops at ~21.7 T. The inset shows the velocity at 70 mK after background subtraction. The frequency

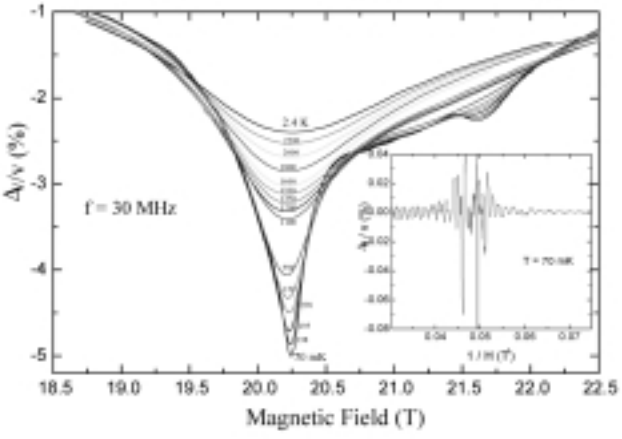

Figure 1. *Relative velocity change at the metamagnetic transition showing a new feature at lower temperatures. Inset shows quantum acoustic oscillations.*

Kondo / Heavy Fermion Systems *continued on page 4*

Kondo / Heavy Fermion Systems ***cont. from page 3***

of the quantum acoustic oscillations increases rapidly as the transition is approached. The high-field frequency (~9.7 MG) is approximately twice the low-field value and does not correspond to any known de Haas-van Alphen orbit. Analysis of the temperature dependence of the oscillation amplitudes at 32 T gives an effective mass ratio of ~31.4.

Acknowledgements: This work was supported by NSF DMR-9704020, 9971123, and 9623682.

Magnetic Resonance Techniques

Development of High Frequency Phased Array Rf Coils

Fitzsimmons, J., *Univ. of Florida Brain Institute (UFBI)/UF, Radiology*
Duensing, R., *UFBI/UF, Radiology*
Peterson, D., *UFBI/UF, Radiology*
Beck, B., *NHMFL/UFBI*

At high field strengths on large samples (humans) it becomes very difficult if not impractical to construct large body rf coils. It becomes difficult to tune the coil and the rf power requirements become excessive. Consequently most high field studies (above 2 T) on humans have concentrated on the brain where smaller coils can be used. There are substantial benefits for high field imaging outside of the brain, however, and suitable rf coil developments are required.

One option is to use phased array coils as commonly used clinically for signal reception. These coils, however, are normally receive only, requiring a body coil for transmission. A potential solution is to make the phased array coils capable of transmission and reception. At UF the first transcieve phased array rf coils were developed at 3 T. A four coil array was developed for imaging the spine. Using this technology the first spinal cord images were obtained on humans at 3 T. These studies are now being extended to other coil types, and we will shortly be funded to develop a transcieve phased array head coil.

This technology was further developed by other workers at UF to construct a pelvic phased array coil for prostate studies (see "Development of Prostate MRI/S Using Transcieve Coils at 3 T" elsewhere in this document), and the technology is being used to develop phased array coils for the present 4.7 T/33 cm and upcoming 11.7 T/40 cm animal systems, presently in the prototype stage.

The rf group is also involved in other rf coil developments for a variety of applications indirectly supported by the NHMFL, including birdcage coils for knee imaging at 3 T[2] and cardiac spectroscopy at 3 T.[3]

Acknowledgements: This work was supported by the NHMFL and UFBI.

1 Duensing, *et al*., ISMRM 6th Annual Meeting (1998).
2 Peterson, *et al*., Magn Reson Med, **42**, 215-221 (1999).
3 Bruner, *et al*., ISMRM 7th Annual Meeting, (1999).

Resolution Enhancement Using CPMG-HOMOGENIZED Detection of Solution NMR on the Keck Magnet

Lin, Y.-Y., *Princeton Univ., Chemistry*
Ahn, S., *Princeton Univ., Chemistry*
Garrett-Roe, S., *Princeton Univ., Chemistry*
Warren, W. S., *Princeton Univ., Chemistry*
Murali, N., *NHMFL*
Brey, W., *NHMFL*
Bowers, C.R., *NHMFL/UF, Chemistry*

Researchers interested in high-resolution NMR spectroscopy have long sought higher magnetic fields to enhance resolution and simplify spectra. Resistive or hybrid magnets can achieve substantially higher static fields than those available in superconducting magnets, but their *spatial uniformity* and *temporal stability* are unacceptable for high-resolution NMR applications.

A recently proposed detection method, termed "homogenized", can remove spatial inhomogeneous broadening while retaining chemical shift differences and scalar couplings.[1] The homogenized sequence is based on observations of intermolecular zero-quantum coherences (iZQC) induced by the distant dipolar field between a solute molecule and solvent

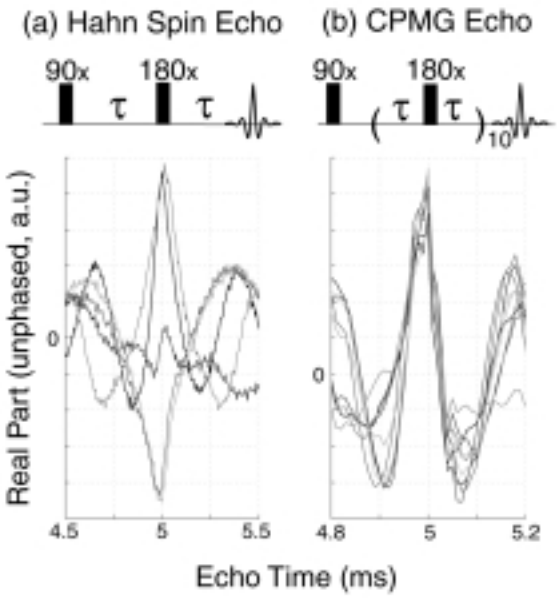

Figure 1. *Spin echo generated by (a) Hahn echo sequence (5 superimposed), and (b) CPMG sequence (10 superimposed).*

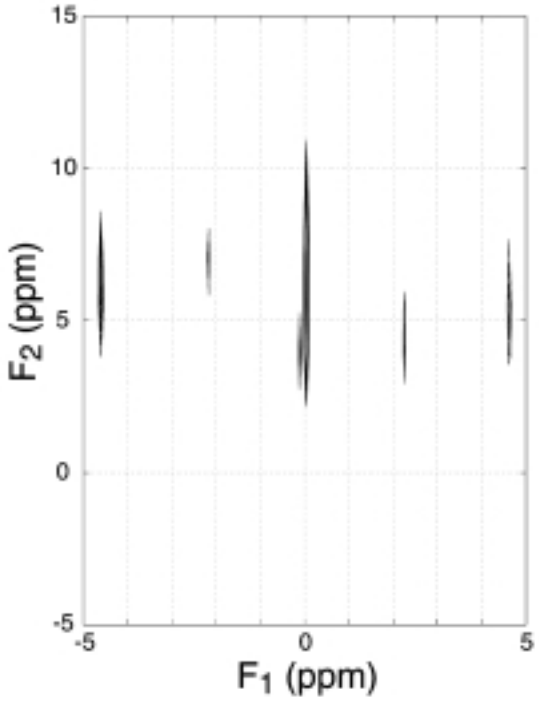

Figure 2. *Experimental iZQC spectrum by CPMG-homogenized sequence.*

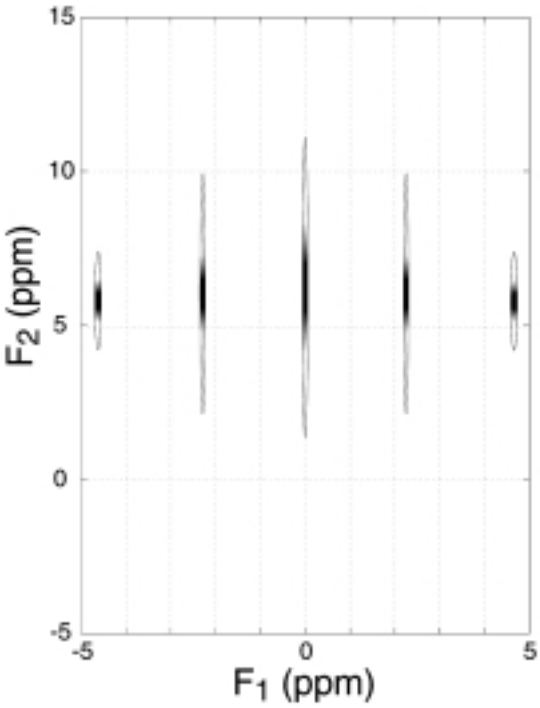

Figure 3. *The corresponding simulated spectrum of Figure 2.*

molecules that are micrometers away. The iZQCs evolve with no inhomogeneous broadening or drift effect, and are converted into solvent magnetization to be detected. For the Keck magnet, drift effects on the observed solvent magnetization must also be eliminated. This can be done with the Carr-Purcell-Meiboom-Gill (CPMG) pulse train shown in Figure 1. Pulse intervals <<1 ms give stable echoes in both phase and amplitude. Experimental effects of a CPMG-homogenized sequence on a 1:1 water/acetone sample are shown in Figure 2. The 1600 Hz linewidth is reduced in the indirectly-detected dimension to approximately 30 Hz, in accord with numerical simulations (Figure 3) based on modified Bloch equations.[3] The iZQC spectrum shows the expected peak at the precise frequency difference with correct phase alternation, plus a peak at twice the difference (which is also expected with this sample.)[2] Consequently, this demonstrates the *first ever high-resolution NMR spectrum* taken at very high magnetic field (>1GHz).

Acknowledgements: This work was supported by NIH and NHMFL.

1 Vathyam, S., *et al*., Science, **272**, 92 (1996).
2 Ahn, S., *et al*., J. Magn. Reson. A., **133**, 266 (1998).
3 Enss, T., *et al*., Chem. Phys. Lett. **305**, 101 (1999).
4 Lin, Y.-Y., *et al*., in preparation for Phys. Rev. Lett.

Magnet Technology

Axisymmetric Ferroshimming of High Field Magnets

Bird, M.D., *NHMFL*

An axisymmetric ferroshim for a high field magnet can be designed by considering a stack of rings of ferromagnetic material of uniform inner diameter located in the bore of the electromagnet. The outer diameter of each ring is a free parameter. The applied magnetic field (>2 T) takes each ring to its saturation magnetization and the field contribution from each ring can be easily computed at any point in space. A non-linear optimization algorithm can then be used to compute the outer diameter of each ring of material to shape the field as desired over some volume of space.

One application of this technology is to increase the uniformity of the field provided by the electromagnet. Such a shim was

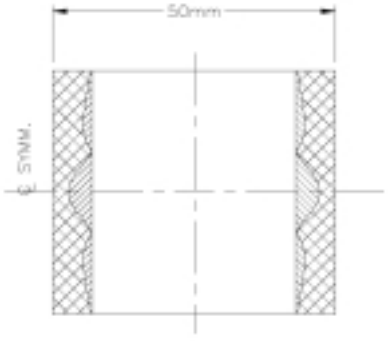

Figure 1. *Profile of ferromagnetic insert for uniform magnetic field. Steel is shown with diagonal hatching, glass-epoxy is shown with cross-hatching.*

Magnet Technology *continued on page 6*

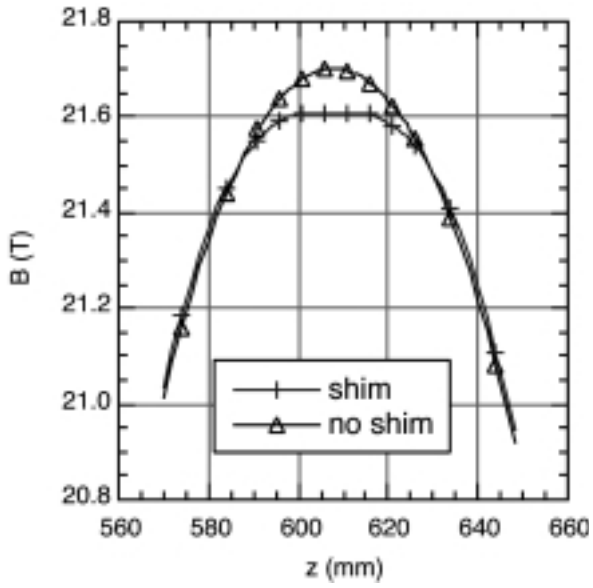

Figure 2. *Measured on-axis field of 27 T magnet with and without high field uniformity insert.*

designed and built to be installed in a 50 mm bore magnet operating at 21.7 T at the NHMFL. Figure 1 shows a section of the shim including the steel and glass-epoxy filler used to keep the shim centered. Figure 2 shows a Hall probe map of the field along the axis both with and without the insert. We see that the inhomogeneity over a 6 mm diameter spherical volume has been reduce by a factor of 4. Such a system is inexpensive and easily installed compared with traditional approaches.

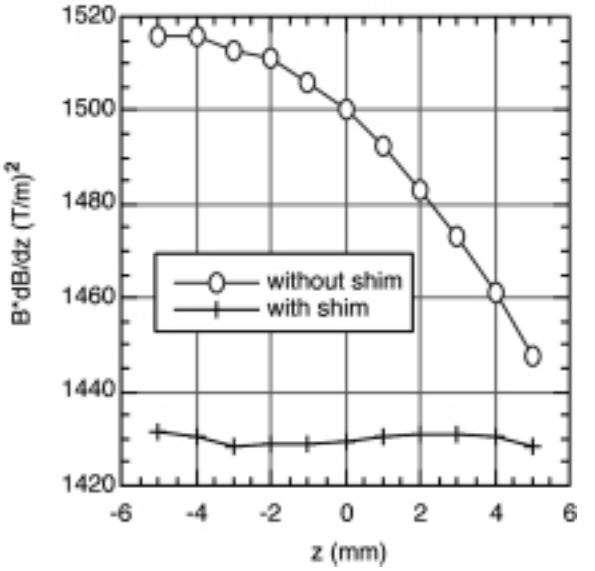

Figure 3. *B_Z*dB_Z/dz computed along the axis of the 27 T, 50 mm bore magnet with and without uniform levitation insert.*

Another application for axisymmetric ferroshims is in providing a space with uniform levitation force. Levitation of most biological materials requires a product of field and field-gradient to be around 1400 T^2/m.[1] While most of the high field resistive magnets at the NHMFL provide greater than this amount, the levitation force can vary by as much as 10% over 5 mm. A second ferroshim has been designed for uniform levitation force and the computed levitation force with and without this insert is presented in Figure 3.

[1] Brooks, J.S., *et al.*, "New opportunities in science, materials, and biological systems in the low-gravity (magnetic levitation) environment," submitted to 44th Conf. on Magn. and Magn. Mat., 1999.

Magnetism & Magnetic Materials

Melting of Charge/Orbital Ordered States in $Nd_{1/2}Sr_{1/2}MnO_3$: Magnetic Field Dependent Optical Studies

Jung, J.H., *Seoul National Univ. (SNU)-Korea, Physics*
Lee, H.J., *SNU-Korea, Physics*
Noh, T.W., *SNU-Korea, Physics*
Choi, E.J., *Univ. of Seoul-Korea, Physics*
Moritomo, Y., *Nagoya Univ.-Japan, Applied Physics*
Wang, Y.J., *NHMFL*
Wei, X., *NHMFL*

Doped manganites with small bandwidths near half doping show intriguing charge ordering phenomena, i.e. real space orderings of the Mn^{3+} and the Mn^{4+} ions. The charge ordering in $Nd_{1/2}Sr_{1/2}MnO_3$ incorporates d_{3x2-r2} (d_{3y2-r2}) orbital ordering and CE-type antiferromagnetic spin ordering. Interestingly, it was found that some charge ordered states could be changed into ferromagnetic metallic states under

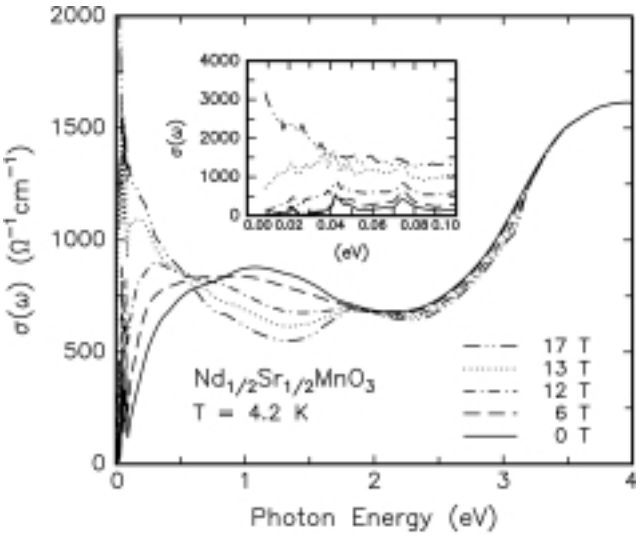

Figure 1. *H-dependent σ(ω) of $Nd_{1/2}Sr_{1/2}MnO_3$. In the inset, σ(ω) below 0.1 eV are shown.*

a high magnetic field.[1] (This transition is usually called "melting" of charge/orbital ordered states.) Although it is a very intriguing phenomenon, its electrodynamics has been rarely investigated.

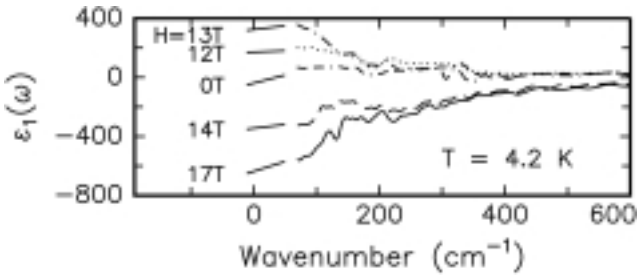

Figure 2. *H-dependent ε_1 of $Nd_{1/2}Sr_{1/2}MnO_3$.*

We measured magnetic field (H = 0 ~ 17 T) dependent optical conductivity spectra $\sigma(\omega)$ of $Nd_{1/2}Sr_{1/2}MnO_3$. The H-dependent $\sigma(\omega)$ at 4.2 K are shown in Figure 1. At 0 T, the spectra show typical features of a charge/orbital ordered insulator with ~ 0.1 eV optical gap. With increasing H, the spectral weights near 1.2 and 2.7 eV are transferred to lower energy regions. The gap values seem to decrease and finally disappear above 13 T. Details of transferred spectral weights below 0.1 eV can be seen in the inset of Figure 1. With increasing H, the phonon modes at 0 T are screened and the Drude peak appears above 13 T. Note that the Drude peak becomes clear and appeared below 0.04 eV. Therefore, $\sigma(\omega)$ of melted states should be viewed as two absorptions i.e., Drude weight and an incoherent peak, similar to ferromagnetic metallic states of colossal magnetoresistance manganites.[2]

To get a better understanding on the insulator-metal transition, we plot the real part of the dielectric constant ε_1 as shown in Figure 2. In the insulating state at 0 T, ε_1 is positive and $d\varepsilon_1/d\omega \approx 0$. With increasing H up to 13 T, ε_1 increases. Above 14 T, it becomes negative and $d\varepsilon_1/d\omega > 0$, which is consistent with metallic responses. To explain this intriguing behavior of ε_1, we applied a composite medium model.[3] The excellent agreement between the experimental data and the theoretical predictions strongly suggests that the melting of charge/orbital ordered states should occur through the percolation of ferromagnetic metal domains.

1 Kuwahara, H., *et al.*, Science, **270**, 961 (1995).
2 Kim, K.H., *et al.*, Phys. Rev. Lett., **81**, 1517 (1998).
3 Noh, T.W., *et al.*, Phys. Rev. B, **33**, 3793 (1986).

Zeeman Effect on de Haas-van Alphen Oscillations in a 2D Magnetic Breakdown System

Han, S.Y., *NHMFL*
Brooks, J.S., *NHMFL/FSU, Physics*
Kim, Ju. H., *Univ. of North Dakota, Physics*

We use a quantum mechanical model to compute magnetic quantum oscillations in two dimensional magnetic breakdown systems. A tight binding model was derived from the actual crystal structure and atomic orbital of α-$(ET)_2KHg(SCN)_4$ according to the extended Hückel prescription. Four bands and seven different transfer integrals replicate the real system. An extra magnetic symmetry generates a Hofstadter[1] type energy spectrum by taking magnetic fields satisfies the condition, the ratio of the magnetic flux per unit cell to the flux quantum (ϕ/ϕ_0) becomes a ratio of integers p/q. From the energy spectrum the field dependent magnetization can be calculated following the standard procedure[2]. As a result, dHvA oscillations with breakdown effect and $f_{\beta-\alpha}$ appeared naturally as an outcome.[3] In this report we present a new result that was obtained by including the non-interacting spin effect in the previously described calculation. Our quantum mechanical results are also compared with the standard Lifshitz-Kosevich (LK) formula.[4]

When non-interacting spins are considered, spin states are orthogonal to other eigen states and spin terms only appear in the diagonal elements of the matrix with the matrix size doubled from the spinless Hamiltonian. The Hamiltonian can be represented by: $H = H_0+H_S$, and $H_S = g\sigma\mu_B B/2$, where σ

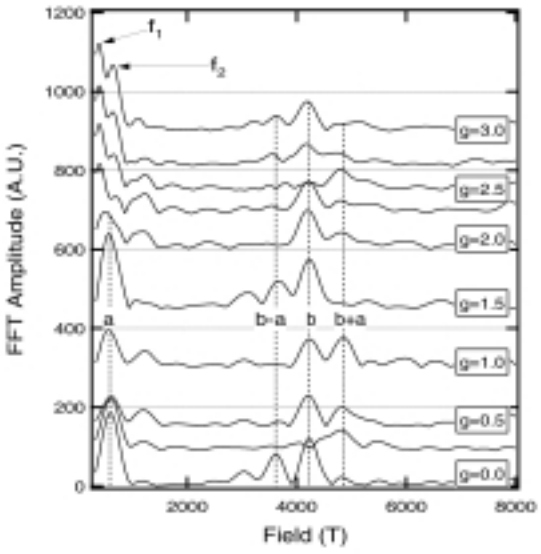

Figure 1. *The FFT spectrums for g between 0 to 3. Curves are offset in proportion to g.*

Molecular Conductors *continued on page 8*

is ±1 and g is the spin splitting factor close to 2. The spin degeneracy is lifted and energy levels linearly split to up and down spin levels. In LK formula the phase difference coming from the linear spin splitting causes a damping factor, R_S in magnetic oscillations, where R_S is proportional to cos(1/2pπgm*). We calculate the magnetization for several g values at a finite temperature close to zero. The dHvA oscillations are Fourier transformed (FFT) in Figure 1. The amplitude of each peak periodically oscillates as a function of g.

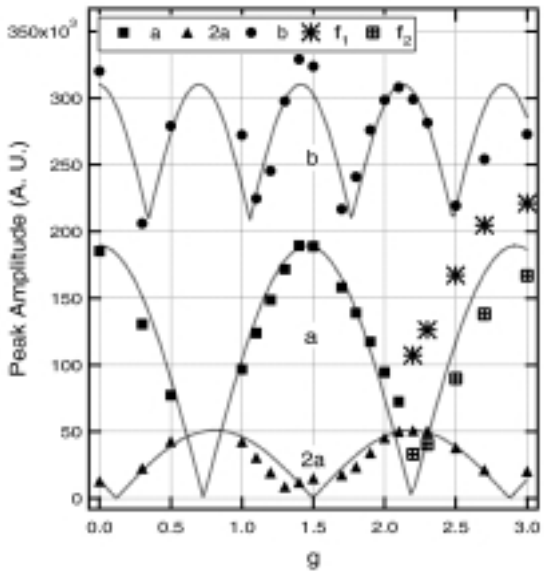

Figure 2. *The FFT amplitudes vs. g and the LK spin term, R_s. The f_1 and f_2 are new frequencies that split from f_α for g > 2.1.*

In Figure 2, peak amplitudes as a function of g are plotted and numerically fitted to the absolute value of R_S. The cosine behavior expected from the LK is confirmed even in these high fields with the existence of the Hofstadter energy substructures. From the LK fitting we also estimated the effective masses. The estimates of effective masses are 1.37 m_e for $m^*{}_\alpha$ and 2.85 m_e for $m^*{}_\beta$. These are close in value to those from the temperature fitting. Another important aspect we obtain from the g dependent FFT result is the splitting of the fundamental frequency at high g values. The fundamental frequency, f_α (599 T) splits into two new frequencies, f1 (382 T) and f2 (626 T). We find that the LK description of the spin damping holds even in systems with a complex energy spectrum and in extremely high magnetic fields.

Acknowledgements: This research was supported by NSF-DMR 99-71474 and 95-10427 (JSB). The NHMFL is supported through a Cooperative Agreement between the NSF through NSF-DMR-95-27035 and the State of Florida.

1 Hofstadter, D.R., Phys. Rev. B, **14**, 2239 (1976).
2 Landau, L.D. and Lifshitz, E.M., *Statistical Physics 3rd edition.* (Course of Theoretical Physics. Vol. 5., 1976).
3 Kim, Ju. H., *et al*., Phys. Rev. B. **60**, 3213 (1999).
4 Lifshitz, I.M. and Kosevich, A.M., Zh. eksp. teor. fiz., **29**, 730 (1955).

Angle Dependence of the Upper Critical Field and Evidence for the Fulde-Ferrell-Larkin-Ovchinnikov State in the Organic Superconductor κ-(BEDT-TTF)$_2$Cu(SCN)$_2$

Symington, J.A., *Univ. of Oxford, Physics*
Nam, M.-S., *Univ. of Oxford, Physics*
Singleton, J., *Univ. of Oxford, Physics*
Ardavan, A., *Univ. of Oxford, Physics*
Blundell, S.J., *Univ. Of Oxford, Physics*
Harrison, N., *LANL*
Mielke, C.H., *LANL*
Kurmoo, M., *Institut de Physique et Chimie des Materiaux de Strasbourg, (IPCMS), France*
Day, P., *The Royal Institution, London, U.K.*

We have performed a detailed study of the dependence of the resistive upper critical field on the direction of the magnetic field B in the organic superconductor κ-(BEDT-TTF)$_2$Cu(NCS)$_2$. [1] The measurements used a special two-axis rotation insert built in Oxford, which allows the sample to be orientated at any angle to B in-situ and at cryogenic temperatures; fields were provided by magnets at Tallahassee, LANL and Oxford. The orientation of the sample is defined by the polar angle θ between B and the normal to the sample's bc planes and the azimuthal angle φ; φ=0 represents a plane of rotation of B containing b and the normal to the bc plane. Figure 1 (upper part) shows the φ dependence of the in-plane(θ=90°) resistive upper critical field defined by a zero magnetoresistance extrapolation ($B_{MR\to0}$) at temperatures of 4.2 K and 1.45 K. There is little or no φ dependence of the critical field in spite of evidence of gap nodes characteristic of d-wave superconductivity.[2,3] Figure 1 (lower part) shows the full θ and φ dependence of $B_{MR\to0}$ at 1.45 K. The θ dependence of the measured critical fields can be described by Eqn. 1, which represents an anisotropic orbital limiting mechanism, combined with an isotropic Pauli paramagnetic limit.[1]

$$B_{c2}(\theta) = \frac{B_0}{\sqrt{\cos^2(\theta) + \alpha^2}} \qquad (1)$$

Here $B_0=(1+\alpha^2)B_{c2}(\theta=0)$, $\alpha=B_0/B_{spin}$, and B_{spin} is the limiting field due to the spin.[1] Eqn. 1 gives a good fit of the θ dependence of $B_{MR\to0}$ for angles $|\theta| \leq 86°$. However, the data for $|\theta|$ closer to 90° do not follow the same dependence, and $B_{MR\to0}$ exceeds both the fitted B_{spin} and the Pauli paramagnetic limit[1] at 1.45 K and at 4.2 K.

It has been suggested[4] that such behavior could indicate the existence of a Fulde-Ferrell-Larkin-Ovchnnikov state, a state in which there is an attractive interaction between carriers

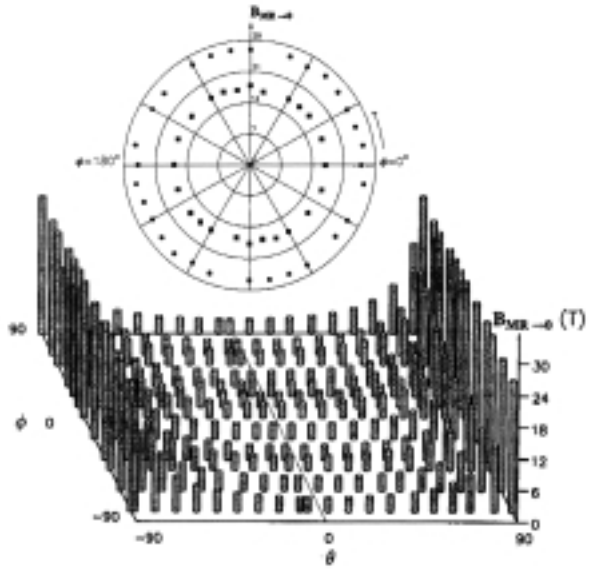

Figure 1. *Upper part: azimuthal angle dependence of in-plane $B_{MR\rightarrow 0}$ at T= 4.2 K (filled squares) and 1.45 K(filled circles) in κ-(BEDT-TTF)$_2$Cu(NCS)$_2$. Lower part: the full angle dependence of $B_{MR\rightarrow 0}$ at 1.45 K.*

with opposite spins on opposite sides of the Fermi surface, which leads to the formation of pairs with non zero total momentum;[5,6] further experiments were therefore carried out to check this proposal.[7] Single crystals were mounted within the coil of a tuned circuit differential susceptometer (TCDS)[7]. In the TCDS, the coil is part of a tuned circuit operating at ~3 MHz. Changes in the magnetization and the differential susceptibility of the sample are detected as shifts in the frequency. The sample magnetoresistance was measured simultaneously. Samples were aligned with the field parallel to the highly conducting planes to within 0.1°.[4] The TCDS frequency is shown in Figure 2 (left side) for temperatures in the range 1.39 K to 4.2 K. The upper critical field was

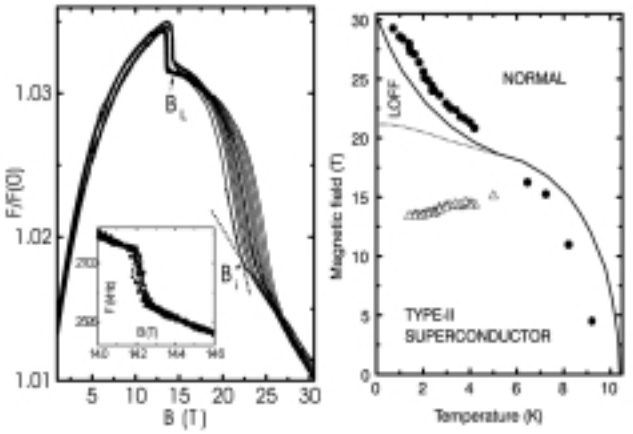

Figure 2, *Left side: the normalized TCDS frequency vs. magnetic field for several temperatures T between 1.39 K and 4.2 K for the field parallel to the highly conducting layers. A sharp drop in frequency is seen at B_L ~ 14 T, moving to lower fields as T decreases. The inflection at higher fields are associated with the upper critical field. The inset shows an enlargement at the region around B_L. Right side; temperature dependence of the fields B_i (triangles) and B_m (circles) compared with the theoretical FFLO phase diagram of Reference 3.*

observed for each temperature as a point of inflection, B_i. The values of B_i agree well with simultaneous measurements of the resistive midpoint fields B_m.[1] However, the most striking feature of the data was a sharp drop, B_L, which remains at ~14 T for all temperatures. The sharpness of this feature suggests that it is a first-order transition.[7]

Figure 2 (right side) shows the temperature dependence of B_m and B_i plotted alongside a theoretical phase diagram for the FFLO state.[4] The data in the figure bear a strong qualitative resemblance to the theoretical phase diagram, as the drop at B_L is indicative of the first order phase transition (c.f. the theoretical first-order phase transition between the superconducting and FFLO states). Moving away from the in-plane geometry allows the number of closed quasiparticle orbits to increase and so orbital mechanisms destroy the superconductivity. The drop in the response of the TCDS is only clearly visible when the field is within 4° of parallel to the conducting layers.

1 Nam, M.-S., *et al*., J. Phys.:Condens. Matter, **11**, L477 (1999).
2 Schmalian, J., Phys. Rev. Lett., **81**, 4232 (1998).
3 Schrama, J.M., *et al*., Phys. Rev. Lett., **83**, 3041 (1999).
4 Shimahara, H., Phys. Rev. B, **50**, 12760, (1994).
5 Fulde, P. and Ferrell, R.A., Phys, Rev., **135**, A550, (1964).
6 Larkin, I. and Ovchinnikov, Y.N., Zh. Eksp. Teor. Fiz, **47**, 1136, (1964).
7 Symington, J.A., *et al*., Phys. Rev. Lett. submitted; APS preprint /eprint/gateway/eplist/aps1999aug23_001.

Quasi-Two-Dimensional Spin-Split Fermi-Liquid Behavior of κ-(BEDT-TTF)$_2$I$_3$

Wosnitza, J., *Universität Karlsruhe, Germany, Physikalisches Institut*
Harrison, N., *NHMFL/LANL*
Qualls, J.S., *NHMFL/FSU, Physics*
Brooks, J.S., *NHMFL/FSU, Physics*
Balthes, E., *Universität Stuttgart, Physikalisches Institut*
Schweitzer, D., *Universität Stuttgart, Physikalisches Institut*

The organic superconductor κ-(BEDT-TTF)$_2$I$_3$ is characterized by an exceptionally pronounced two dimensionality (2D) of his electronic bandstructure. While the behavior of the magnetic quantum oscillations in this material conforms mostly to standard models at low magnetic fields,[1] strong deviations from these models, i.e., an apparent reduction of the effective mass, were observed in Shubnikov–de Haas (SdH) experiments at higher magnetic fields.[2]

We measured both the magnetization and the magnetoresistance in pulsed magnetic fields extending to 60 T and in static fields up to 20 T at very low temperatures down to 30 mK.[3] Figure 1a shows an example of an induced voltage signal. The Fourier transformation of the data below 40 T (Figure 1b) displays a dHvA frequency of 575 T corresponding

Molecular Conductors *continued on page 10*

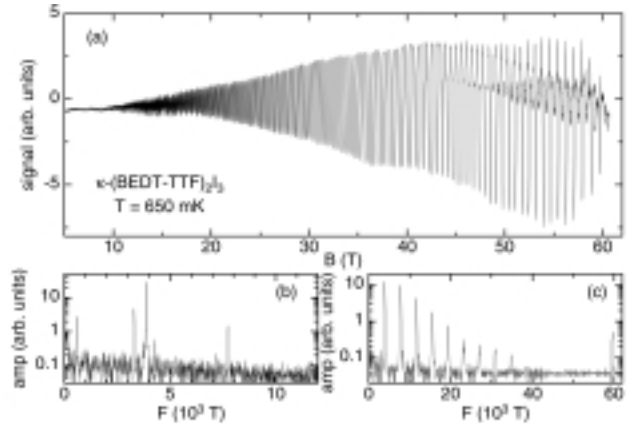

Figure 1. *(a) Raw signal detected on the falling side of a magnetic field pulse. The Fourier transformations in 1/B space for the field intervals 10 < B < 40 T (b) and 40 < B < 61 T (c).*

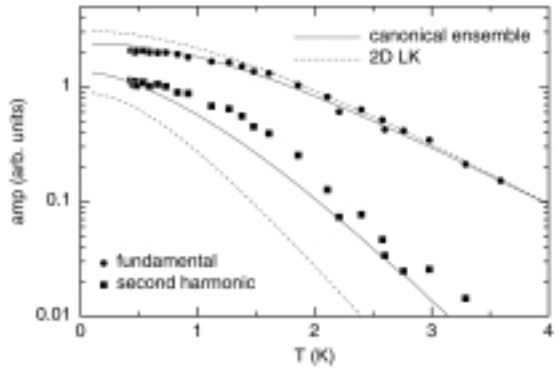

Figure 2. *A comparison of the temperature dependences of the measured dHvA amplitudes with results using a numerical model (solid lines) and the LK theory.*

to the so-called α pocket of the Fermi surface (FS) and the much larger frequency of 3875 T due to the breakdown β orbit. In many ways the oscillations below about 40 T reproduce the behavior seen in previous studies, with the exception of a β–α frequency which might be due to the oscillatory chemical potential in this 2D material. At higher magnetic fields the salt is taken deep into the magnetic-breakdown regime with a rich harmonic content of the oscillations and finally a double-peak structure developing (Figure 1c). The latter structure is a result of well-resolved spin-split Landau levels in strong magnetic fields.

In contrast to the SdH effect, the oscillatory magnetization is a thermodynamic function of state, and is therefore able to probe the Fermi-liquid ground state directly. From the measured temperature dependences of the dHvA-oscillation amplitudes in pulsed field down to 0.4 K and in static fields down to 30 mK we obtain lower-than-expected effective masses when we fit the usual Lifshitz–Kosevich (LK) temperature reduction factor. At lower fields and higher temperatures the low-field value $m_c = 3.9\ m_e$[1] is extracted. While the sign of the apparent mass change is in agreement with our and previous SdH studies,[2] this change is much more acute in the SdH signal. Deviations from the LK behavior due to a fixed chemical potential can be calculated quantitatively by use of a numerical model.[4] In the present case the effect of spin splitting is prominent and has to be taken into account properly. Figure 3 shows our experimental data for the fundamental and second harmonic of the dHvA amplitudes in comparison to the relative temperature dependences obtained from the numerical calculations by use of parameters extracted at low fields (solid lines) and with those of the LK theory (dashed lines). The numerical model describes the experimental dHvA data perfectly well.

1 Heinecke, M., *et al*., Z. Phys. B, **93**, 45 (1993).
2 Balthes, E., *et al*., Z. Phys. B, **99**, 163 (1996); Synth. Metals 94, 3 (1998).
3 Harrison, N., *et al*., Phys. Rev. B, **58**, 10248 (1998).
4 Harrison, N., *et al*., Phys. Rev. B, **54**, 9977 (1996).

Other Condensed Matter

High Field Shubnikov-de Haas Oscillations in Electrodeposited Bi Single Crystal Films

Li, Y., *FSU, Center for Materials Research and Technology (MARTECH)*
Parker, J.S., *FSU, MARTECH*
Xiong, P., *FSU, MARTECH*
von Molnár, S., *FSU, MARTECH/NHMFL*
Yang, F.Y., *Johns Hopkins Univ., Physics*
Chien, C.L, *Johns Hopkins Univ., Physics*

Bismuth is the archetypal semi-metallic system in which quantum magnetotransport effects were first observed. Single crystals of the material exhibit large, positive magnetoresistance (MR) because of the long mean free paths

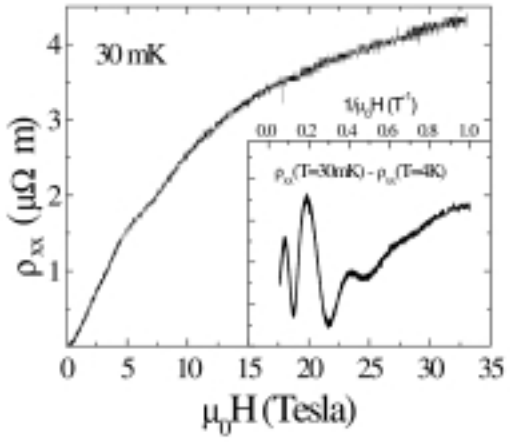

Figure 1. *Magnetoresistance (MR) at 30 mK of a single crystal thin film of Bi produced by electrodeposition. The inset shows the Shubnikov-de Haas oscillations obtained by subtracting the 4 K MR data from the 30 mK data, which are periodic in inverse field.*

of the multiband carriers. If high quality thin films of the material can be fabricated, it may be possible to use them as high field, magnetoresistive sensors. Normal thin film growth methods, however, have resulted in granular, polycrystalline films that inhibit the carrier mean free paths.

Recently, single crystal thin films have been fabricated by electrodeposition.[1] We have performed MR and Hall measurements on Bi films grown by this method onto Si with an Au buffer layer, in both the superconducting magnet (18 T) and a resistive magnet (33 T), at a temperature down to 30 mK. The MR was measured in three different orientations, taking advantage of the in-situ sample rotator. The perpendicular field orientation, with H along (111), is shown in Figure 1. Shubnikov-de Haas (SdH) oscillations are a low temperature phenomenon, while the positive MR is insensitive to temperature in the residual resistivity regime. Therefore, the oscillations may be isolated by subtracting MR data obtained at 4.2 K from the 30 mK data; this is shown in the inset to Figure 1, where the data is plotted vs. inverse field since SdH is periodic in inverse field. Clear oscillations were observable in both the MR and the Hall effect data, attesting to the high quality of these films.

[1] Yang, F.Y., *et al*., Science, **284**, 1335 (1999).

Magnetic Alignment of Carbon Nanotubes

Walters, D.A., *Rice Univ., Center for Nanoscale Science and Technology (CNST)*
Casavant, M.J., *Rice Univ., CNST*
Qin, X.C., *Rice Univ., CNST*
Schmidt, J., *Rice Univ., CNST*
Huffman, C.B., *Rice Univ., CNST*
Haroz, E.H., *Rice Univ., CNST*
Smith, K., *Rice Univ., CNST*
Colbert, D.T., *Rice Univ., CNST*
Smalley, R.E., *Rice Univ., CNST*

Single-wall carbon nanotubes[1] have a broad range of potential applications due to their exceptional mechanical, thermal, electronic, and optical properties. To date, these properties have been studied primarily using mats of randomly oriented nanotubes, obscuring the true anisotropic behavior of the nanotubes. Theory[2] has predicted that nanotubes will be more diamagnetic when oriented perpendicular to a magnetic field than when parallel to it. Therefore, the magnetic energy $U=-\boldsymbol{m}\cdot\boldsymbol{B}$ of a freely rotating nanotube will be minimized when its axis is aligned with the field direction. To achieve alignment, the field must be strong enough that the alignment energy is many times the thermal energy k_BT.

Using the 19 T, 198 mm bore resistive magnet at the NHMFL, we measured the optical transmittance of a colloidal suspension of nanotubes as a function of polarization angle and field

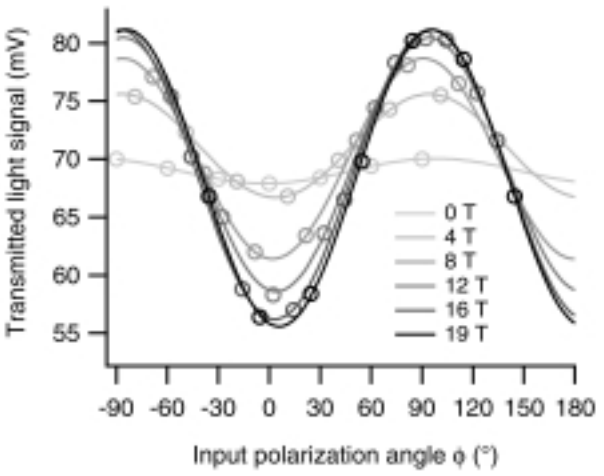

Figure 1. *Optical transmittance at λ = 633 nm of a suspension of single-wall carbon nanotubes. The sinusoidal variation with ϕ indicates that nanotubes are aligned parallel to the magnetic field. The effect saturates at a peak-to-peak-modulation of almost 40%, due to the excellent alignment achieved in high fields. Note: the angle ϕ = 0° corresponds to incident polarization parallel to the field direction.*

(Figure 1). The sinusoidal polarization dependence at fields >4 T is evidence for magnetic alignment of the nanotubes. The amplitude of the sinusoid saturates at the highest fields; our model reveals that the alignment energy of the nanotubes at 19 T is (28 ± 3) times thermal energy at room temperature.

To study further the properties of aligned nanotubes, we assembled them into a solid layer by filtration in a magnetic field parallel to the filter membrane surface. Upon drying, the resulting film could be peeled off the filter membrane. It cleaved readily into long ribbons with edges parallel to the magnetic field direction (Figure 2), demonstrating that

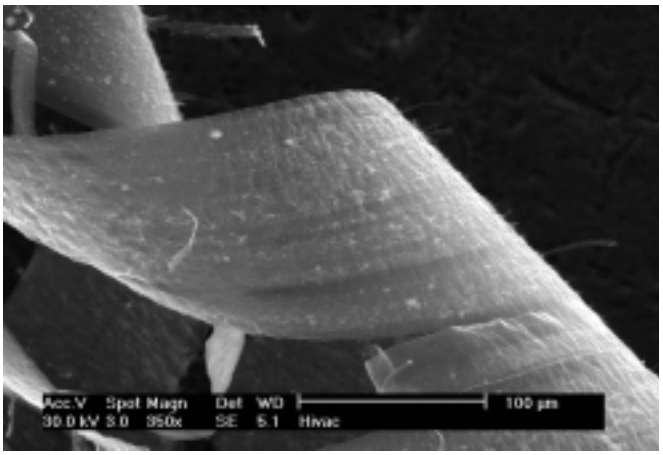

Figure 2. *Ribbon of the novel aligned nanotube solid material produced upon filtering a colloidal suspension of nanotubes in a magnetic field of 25 T. Due to the high degree of organization, the material cleaves along lines parallel to the magnetic field. This material holds great promise for studying, in a bulk assembly, the anisotropic properties of nanotubes.*

Other Condensed Matter *continued on page 12*

it consists of long ropes of nanotubes that are well-oriented parallel to the field. Ongoing experiments are exploring the electronic and optical properties of this novel material. It may even be capable of acting as a seed crystal for the growth of continuous nanotube cables and fibers.

Acknowledgements: This work was supported by the Office of Naval Research (#N00014-99-1-0246), the National Aeronautics and Space Administration (#NCC 9-77), and the Welch Foundation.

1 Thess, A., *et al.*, Science, **273**, 483 (1996).
2 Lu, J.-P., Phys. Rev. Lett., **74**, 1123 (1995).

Quantum Solids

Magnetism of ^{3}He Nano-Clusters in a ^{4}He Matrix

Adams, E.D., *UF, Physics*
Matsunaga, N., *UF, Physics*
Schuberth, E.A., *Walther Meissner Institut*
Shvarts, V.A., *UF, Physics/NHMFL*
Xia, J.S., *UF, Physics/NHMFL*

Simultaneous measurements of susceptibility and pressure have been made in ^{3}He nano-clusters, formed after phase separation of the initial ^{3}He-^{4}He mixture, at temperatures down to 0.5 mK. Pressures were in the range of 3.0 to 3.6 MPa, which produce three different, unique environments for the nano-clusters. At the highest pressure, which is above the melting pressure of pure bulk ^{3}He, the nano-clusters are completely solid, as observed from the pressure measurements. At pressures near 3.0 MPa, the ^{3}He forms as liquid droplets when the phase separation occurs, since the pressures is lower than of pure bulk ^{3}He. Upon cooling to lower temperatures, nano-clusters formed at intermediate pressures undergo partial melting, as observed by the pressure. Susceptibility measurements, using pulsed NMR, of the nano-clusters have been made in all three of these situations, with the temperature measured by pure ^{3}He melting pressure.

The sample studied most extensively was at a pressure of 3.36 MPa, which was observed to undergo partial melting at about 20 mK. From the change in pressure on partial melting, it was determined that a large fraction of the cluster did not melt. One possible explanation for this is that the van der Waals attraction by the more dense ^{4}He produces a dense layer of ^{3}He at the interface that remains solid, with only the center of the cluster undergoing melting. In contrast to pure bulk solid ^{3}He at this pressure, which orders antiferromagnetically at about 0.9 mK, this sample followed a Curie law, $\chi = C/T$, (with a negligible Weiss θ) to the lowest temperature of about 0.5 mK.

The sample at a pressure 3.5 MPa, which showed no melting since it was above the melting pressure of pure bulk ^{3}He, also deviated very little from the Curie law above 1 mK. At lower temperatures, however, there was a gradual increase of χ above the Curie behavior, indicating a tendency toward ferromagnetism. These preliminary results, which have been reported previously,[1-3] must be investigated further.

1 Adams, E.D., *et al.*, J. Low Temp. Phys., **113**, 375 (1998).
2 Matsunaga, N., *et al.*, Proc. LT-22, August 1999, Helsinki, Finland.
3 Adams, E.D., *et al.*, Invited oral presentation, QFS-99, August 1999, St. Petersburg, Russia.

NMR Studies of Quantum Tunneling in a 2D Film of ^{3}He Atoms

Parks, C., *UF, Physics*
Stachowiak, P., *UF, Physics/Univ. of Wroclaw*
Sullivan, N.S., *UF, Physics/NHMFL*

Pulsed NMR studies at moderately high magnetic fields have been carried out to determine the quantum tunneling regime for a triangular lattice of helium three atoms. Boron nitride powder was used as a substrate and adsorption isotherm studies indicated that atomically clean surfaces could be prepared by suitable baking in a high vacuum. The nuclear spin-spin relaxation times, T_2, were measured for a range of atomic coverages varying from a fraction of the $\sqrt{3}$ X $\sqrt{3}$ commensurate coverage to 20% beyond full monolayer coverage (incommensurate). The values of T_2 are very sensitive to the atomic motion, and in the temperature range where quantum tunneling occurs one expects to observe a temperature independent T_2.[1] Analysis of the value of T_2 in terms of the spectral densities of the motion yields the value of the atom-atom exchange rates.

We have measured T_2 from 120 to 2400 mK and observe a temperature independent plateau from 300 to 1200 mK for coverages near the expected commensurate $\sqrt{3}$ X $\sqrt{3}$ density. We therefore interpret the results as indicating that the relaxation mechanism in this region is determined by the modulation of the dipole-dipole interactions by atom-atom exchange resulting from quantum tunneling. Further studies in the middle of this temperature range were carried out for a series of surface densities. The results showed a remarkable singularity with a sharp reduction in the value of T_2 by a factor of 10 near the completion of the monolayer coverage. This result is attributed to the effect of the mobility of a small number of excess atoms or vacancies with respect to perfect coverage on either side of the perfect monolayer coverage. The observed density dependence provides a measure of the isothermal compressibility of the lattice in analogy to the Grüniesen constant for exchange in 3D samples. The observation is critically important for calibrating the surface of the sample to be certain of the monolayer coverage.

In addition we observe a small peak in the value of T_2 at the exact $\sqrt{3}$ X $\sqrt{3}$ commensurate lattice coverage. This result indicates that the atomic mobility is maximum for this perfect lattice density, and it is these values that are used to determine the mean atomic quantum tunneling rate for a triangular lattice. Experiments are planned to attempt to determine the difference between 3-fold and 2-fold cyclic tunneling rates for this system.

1 Sullivan, N.S. and Chapellier, M., J. Phys. C (Solid State), **7**, L195-197 (1974).

Superconductivity - Basic

Enhancement of the Upper Critical Point in Heavy Ion Irradiated $YBa_2Cu_3O_{7-d}$

Kwok, W.K., *Argonne National Laboratory (ANL)*
Olsson, R. J., *ANL*
Karapetrov, G., *ANL*
Paulius, L.M., *Western Michigan Univ., Physics*
Moulton, W.G., *NHMFL/FSU, Physics*
Hofman, D.J., *ANL*
Crabtree, G.W., *ANL*

The upper critical point was investigated in untwinned $YBa_2Cu_3O_{7-d}$ single crystals with dilute columnar defects. A series of crystals were irradiated at Argonne's Tandem Linear Accelerator System (ATLAS) with 1.4 GeV $^{208}Pb^{56+}$ to a dose matching field of B_Φ=50 G, 100 G, 500 G, and 1000 G. The vortex lattice melting transition was characterized with transport measurements up to H=17 T || c at the NHMFL in Tallahassee. Figure 1 shows the temperature dependence of the superconducting resistive transition for the B_Φ=1000 G crystal and compares it with an unirradiated reference crystal

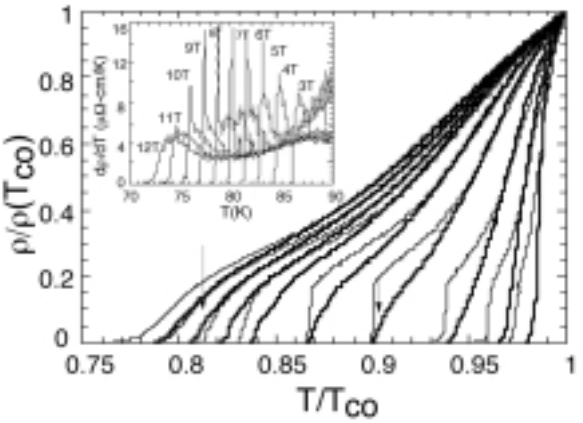

Figure 1. *Temperature dependence of the resisitivity for the unirradiated (thin lines) and irradiated (thick lines) crystals for H=0.5, 1, 2, 4, 6, 8, 9, 10, and 11 T parallel to the c-axis. Inset: Temperature derivative of the resistivity for the irradiated crystal.*

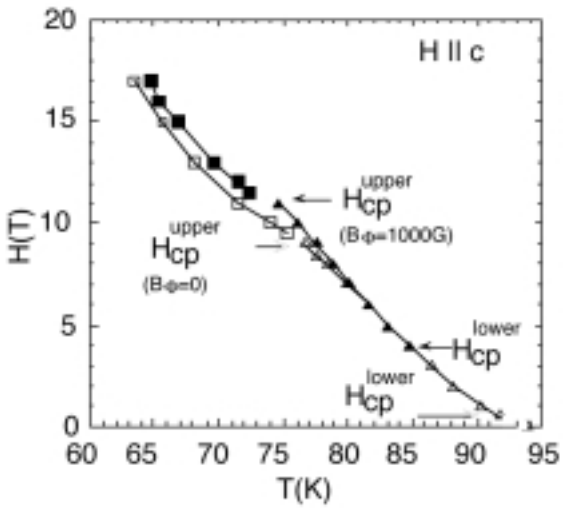

Figure 2. *Superconducting phase diagram depicting the upper and lower critical points of the first order vortex melting transition in the unirradiated (open symbols) and irradiated (closed symbols) crystals.*

cleaved from the same sample. The sharp kink in the resistivity for the unirradiated crystal is associated with the first order vortex lattice melting transition and is observed from 0.5 T up to about 9 T where it disappears. For the irradiated crystal, we observe a similar kink in the resistivity starting near 4 T and extending to beyond 10 T, as shown by the arrows in Figure 1. First order melting is clearly demonstrated in the inset to Figure 1 where we show the temperature derivative of the resistivity for the irradiated crystal. The peaks in dρ/dT reflect the kink in the resistivity at the first order melting transition.

Figure 2 shows the phase diagram of the melting transition determined from the temperature derivative of the resistivity. First order vortex melting occurs in the region between the upper and lower critical points and is shown by triangles. Above the upper critical point, the squares represent the locations of the resistive zeros. For the first time, we report on a dramatic upward shift in the upper critical point from H_{ucp}=9 T to H_{ucp}=11 T after irradiation. We interpret this effect as due to the line-like longitudinal geometry of the columnar defect, which reduces the transverse wandering and entanglement of the vortices. This effect tends to increase the order of the lattice state, and stabilizes it against entanglement to higher fields. The increase in the upper critical point by columnar defects provides direct experimental evidence that entanglement is a key feature of the high field disordered state. Since point defects promote vortex line meandering, the addition of a few columnar defects suppresses the meandering, resulting in an enhancement of the upper critical point.

Superconductivity - Basic *continued on page 14*

Low Temperature Normal State of the High T_c $Bi_2Sr_{2-x}La_xCuO_{6+\delta}$ Revealed by 60 T Magnetic Fields

Ono, S., *CRIEPI, Japan*
Ando, Y., *CRIEPI, Japan*
Murayama, T., *CRIEPI, Japan*
Balakirev, F.F., *NHMFL/LANL*
Betts, J.B., *NHMFL/LANL*
Boebinger, G.S., *NHMFL/LANL*

We investigated transport properties of $Bi_2Sr_{2-x}La_xCuO_{6+\delta}$ (Bi-2201) high-T_c cuprate down to 0.5 K over a wide range of carrier concentrations by suppressing the superconductivity with 60-T pulsed magnetic fields. It was found previously that in the hole-doped $La_{2-x}Sr_xCuO_4$ (LSCO) system a metal-to-insulator (MI) crossover in the normal state takes place exactly at the optimum doping.[1,2] More recently, similar findings were reported for the electron-doped $Pr_{2-x}Ce_xCuO_{4+\delta}$ (PCCO) system.[3] Whether MI crossover is universally associated with the optimum doping in high-T_c cuprates is an important question, in particular for the so-called quantum critical point model of the high-T_c cuprates.

Bi-2201 is a hole-doped high-T_c compound in which the carrier concentration can be varied in a wide range, from the overdoped to the underdoped region[4], which makes it an attractive system for the study of the low-temperature MI crossover. The single crystals of $Bi_2Sr_{2-x}La_xCuO_{6+\delta}$ are grown for this experiment using a floating-zone technique for a wide range of La concentration x, from x=0.23 (overdoped) to 0.84 (heavily underdoped).[4] The resistivity is measured in the transverse geometry, with current along the Cu-O plane and magnetic field along the c-axis (I || ab, B || c). Figure 1 shows the T dependence of ρ_{ab} in 0 T and 60 T, for six x values (x=0.23, 0.39, 0.66, 0.73, 0.76 and 0.84). The x=0.39 sample is optimally doped with $T_c \sim 38$ K.

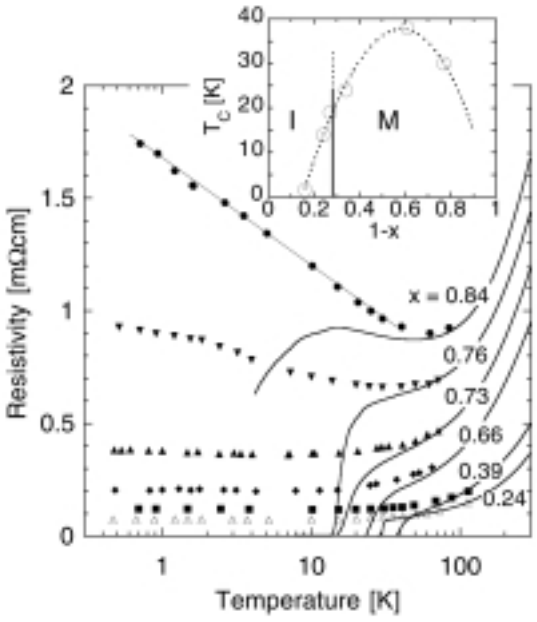

Figure 1. *T dependence of ρ_{ab} of the $Bi_2Sr_{2-x}La_xCuO_{6+\delta}$ crystals in 0 T (solid lines) and 60 T (symbols). The straight line emphasizes the log (1/T) behavior. Inset: Phase diagram of T_c versus 1-x, in which the MI boundary is schematically shown.*

In zero field, all the samples are metallic ($d\rho_{ab}/dT > 0$) except for the x=0.84 sample. When we apply the 60 T field and completely suppress the superconductivity, the metallic behavior gradually changes to an insulating one ($d\rho_{ab}/dT < 0$) with decreasing carrier concentration (increasing x). Thus, the MI crossover in the BSLCO system is more gradual than that in the LSCO system.[1,2] A salient feature here is that a metallic behavior is found in an underdoped sample and therefore the MI crossover lies in the underdoped region, not at the optimum doping. This result is notably distinct from that reported for LSCO[1] or for PCCO[2], indicating that the metal-to-insulator crossover in cuprates is not universally associated with the optimum doping. We also note that $\rho_{ab}/(T)$ of the most underdoped sample (x=0.84) increases as log (1/T) with decreasing temperature for over almost two decades in temperature which bears essential similarity with the still unexplained log (1/T) behavior reported for underdoped LSCO.[1]

1 Ando, Y., *et al*., Phys. Rev. Lett., **75**, 4662 (1995).
2 Boebinger, G.S., *et al*., Phys. Rev. Lett. ,**77**, 5417 (1996).
3 Fournier, P., *et al*., Phys. Rev. Lett., **81**, 4720 (1998).
4 Ando, Y., *et al*., Phys. Rev. B, **60**, R6991 (1999).

High Magnetic Field NMR Study of the d-Wave Vortex in the Overdoped High-T_c Superconductor

Zheng, G.-Q, *Osaka Univ., Physical Science*
Moulton, W.G., *NHMFL*
Kuhns, P., *NHMFL*
Reyes, A.P, *NHMFL*
Clark, W.G., *Univ. of California at Los Angeles, Physics and Astronomy*

The unconventional nature of the superconductivity in the high-T_c cuprates is of great interest. The most prominent difference between conventional superconductors and the high temperature superconductors is that in the latter the order parameter of the Cooper pairs is anisotropic, very likely of d-wave symmetry. This anisotropy leads to the unusual physical properties of the superconducting state. Most thermodynamic quantities exhibit power-law temperature dependence, instead of the exponential one that is seen in conventional superconductors. It also has great significance on the formation of structure of vortices, both topologically and electronically. In a conventional

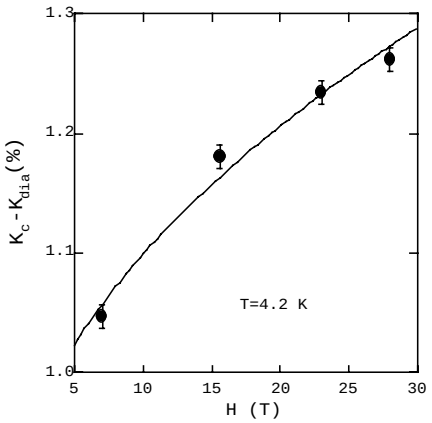

Figure 1. *Magnetic field dependence of the Knight shift at T = 4.2 K.*

s-wave superconductor, the quasiparticle associated with a vortex is confined in the cylinder with diameter of ξ (ξ is the size of the Cooper pairs), and the energy spectrum is discrete, separated by Δ_0^2/E_F where Δ_0 is the maximum of the order parameter or energy gap and E_F is the Fermi energy. For high-T_c superconductors, this energy spacing would be of the order of 50 K if one applied this conventional theory. However, ξ in the high-T_c superconductors is anisotropic because the order parameter is. This may result in an extended quasiparticle state far outside the core center and moreover with the ungapped energy spectrum.

In the present study on an overdoped high-T_c cuprate $TlSr_2CaCu_2O_7$ (T_c = 60 K) under magnetic fields up to 28 T, we have investigated the electronic structure associated with a vortex by measuring the magnetic field dependence of the spin Knight shift, which is proportional to the density of states (DOS). Figure 1 shows the field-induced increase of the ^{63}Cu spin Knight shift at low temperatures as a function of H. The Knight shift is increased markedly by the field, which is not seen in an s-wave superconductor. This result is similar to what we have found previously in an underdoped high-T_c superconductor $YBa_2Cu_4O_8$,[1] but the field effect is much larger. The curve is a fit to K_c-$K_{dia} = K_{orb}+K_s\sqrt{H}$. This result indicates that the field induces a finite DOS around a vortex, which is consistent with the theoretical prediction by Volovik for a d-wave superconductor.[2]

This work was done in collaboration with H. Ozaki, Y. Kitaoka, T. Kondo, Y. Shimakawa and Y. Kubo.

1 Zheng, G.-Q. *et al*, Phys. Rev., B, **60**, R9947 (1999).
2 Volovik, G.E., JETP Lett. **58**, 469 (1993).

Semiconductors

Strongly Anisotropic Electronic Transport at ν = 9/2 and 5/2 under a Tilted Magnetic Field

Pan, W., *Princeton Univ., Electrical Engineering/NHMFL*
Du, R.R., *Univ. of Utah, Physics/NHMFL*
Stormer, H.L., *Columbia Univ., Physics and Applied Physics/ Bell Labs, Lucent Technologies*
Tsui, D.C., *Princeton Univ., Electrical Engineering*
Pfeiffer, L.N., *Bell Labs, Lucent Technologies*
Baldwin, K.W., *Bell Labs, Lucent Technologies*
West, K.W., *Bell Labs, Lucent Technologies*

In higher Landau levels (ν > 4) at half-filling of either spin level (ν = 9/2, 11/2, 13/2, 15/2, etc.) the Hall resistance, R_H, is erratic and diagonal resistance, R, exhibits a strongly anisotropic behavior, showing a strong peak in one current direction (R_{xx}) and a deep minimum when the current direction is rotated by ~90° within the plane (R_{yy}). The origin of these states remains unclear. They are believed to arise from the formation of a striped electronic phase or an electronic phase akin to a liquid crystal phase. We have performed tilted magnetic field experiments in a single-subband heterojunction on the states at these fillings and observed very different behavior for different states.[1] For the states at ν = 9/2 and 11/2, the initial direction of the in-plane anisotropy is overwritten by the in-plane field, B_{ip}. Depending on the tilt direction, and therefore the direction of the in-plane field, the easy direction and the hard direction either remain in place or trade places with increasing B_{ip} [Figure 1(a) and 1(c)]. Surprisingly, the ν = 5/2 and 7/2 states, which do not show any initial in-plane anisotropy become strongly anisotropic under tilt [Figure 1(b) and 1(d)], similar to the states at ν = 9/2 and ν = 11/2. In all cases, under high tilt angles, it is exclusively the relative direction of current and in-plane magnetic field that determines whether R shows a minimum or a maximum.

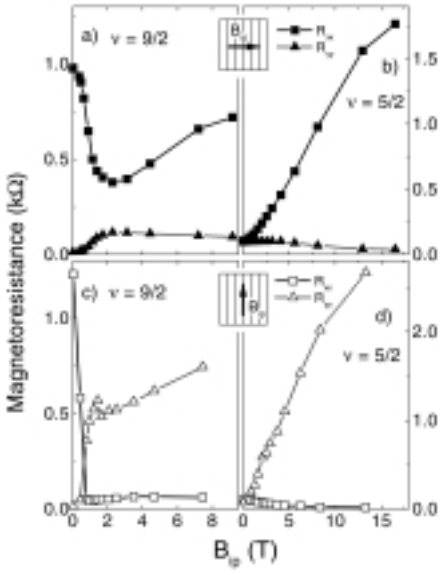

Figure 1. *R_{xx} and R_{yy} as a function of in-plane magnetic field, B_{ip}, at ν = 9/2 and 5/2 for two tilt directions.*

1 Pan, W., *et al*., Phys. Rev. Lett., **83**, 3530 (1999).

REPORTS

The National High Magnetic Field Laboratory

INSIDE THIS ISSUE

Winter 2000 Volume 7 • No. 1

Published by :

National High Magnetic Field Laboratory
1800 East Paul Dirac Drive
Tallahassee, Florida 32310
850-644-0311

Director
Jack Crow

Deputy Director
Hans Schneider-Muntau

Director, Governmental & Public Relations
Janet Patten

Editor/Writer
Kathy Hedick

Design/Production
Educational Media
Walter Thorner
Laurie Anne Lusk

This document is available upon request in alternate formats for individuals with print-related disabilities. Contact Kathy Hedick for more information.

If you would like to be added to our mailing list please write us at the address above, call 850-644-6392, or e-mail hedick@magnet.fsu.edu.

From the Chief Scientist's Desk:
Previewing the 1999 NHMFL
Annual Research Review 1

Selected Reprints
- Biology 1
- Chemistry 1
- Geochemistry 2
- Kondo / Heavy Fermion Systems 3
- Magnetic Resonance Techniques 4
- Magnet Technology 5
- Magnetism & Magnetic Materials 6
- Molecular Conductors 7
- Other Condensed Matter 10
- Quantum Solids 12
- Superconductivity–Basic 13
- Semiconductors 15

REPORTS
The National High Magnetic Field Laboratory

Operated by: FLORIDA STATE UNIVERSITY • UNIVERSITY OF FLORIDA • LOS ALAMOS NATIONAL LABORATORY

1800 East Paul Dirac Drive
Tallahassee, Florida 32310